Precision Engineering 64 (2020) 113–121

Contents lists available at ScienceDirect

Precision Engineering

journal homepage: http://www.elsevier.com/locate/precision

Fabrication of structurally colored basso-relievo with modulated elliptical vibration texturing

Jianjian Wang [a,b], Yaoke Wang [a], Yang Yang [b], Ru Yang [a], Wei-Hsin Liao [b], Ping Guo [a,*]

[a] Department of Mechanical Engineering, Northwestern University, Evanston, IL, USA
[b] Department of Mechanical and Automation Engineering, Chinese University of Hong Kong, China

ARTICLE INFO

Keywords:
Elliptical vibration texturing
Basso-relievo
Structural coloration
Surface texturing
Diffraction grating
Diamond machining

ABSTRACT

Elliptical vibration texturing is a newly arising method for the fast and cost-effective generation of near-subwavelength micro-structures on metal surfaces. This study proposes a fabrication method for structurally colored basso-relievo by combining the surface sculpturing and elliptical vibration texturing in one-step machining. Synergistic modulations of both nominal cutting speed and depth-of-cut (*DOC*) in elliptical vibration texturing are applied to provide concave-convex topography and structural coloration. A new rendering strategy for the face turning configuration with an equidistant spiral tool path has been presented to improve the image rendering efficiency over the raster scan tool path. In addition, different from the conventional elliptical vibration texturing, the nominal *DOC* dynamically changes pixel by pixel in the proposed new process. In order to identify the effects of *DOC* and elliptical vibration trajectories on the surface quality and fidelity of generated gratings, grooving experiments have been conducted on brass samples to further the understanding of nonlinear tool-workpiece interactions. Finally, both raster scan and face turning tests have been performed on an ultra-precision platform with optimized process parameters. Structurally colored basso-relievos with high quality have been successfully demonstrated using the proposed fabrication method.

1. Introduction

Basso-relievo refers to the sculptural relief with a very shallow image raised from the background. Colored basso-relievos fabricated on metallic surfaces are well-received for functional decoration. The fabrication of colored basso-relievos usually relies on a multi-step process sequence to create concave-convex topography and to color the surface separately. The concave-convex low relief is first sculptured by micro-milling [1]. The surface color is then added through plating or pigment painting. In addition to pigmented coloration, structural coloration is another widely adopted principle of color production in nature [2], which utilizes micro/nano-structured surfaces to manipulate the visible light through diffraction, interference, and scattering [3]. Structural coloration shows unique visual effects compared with pigmented coloration; it is more dazzling, brighter, and often has the viewing-angle dependent iridescent effect [4]. Inspired by nature, structural coloration has an array of breakthrough applications in decorative art, anti-counterfeiting, information storage, etc. [5]. It is promising to apply structural coloration to the colored basso-relievo for new functional performances.

To provide structural coloration, various manufacturing technologies have been demonstrated to be capable of fabricating micro/nano-structures on metallic surfaces, which can be divided into two main categories, namely the mechanical and non-mechanical based approaches. In mechanical removal processes, diamond ruling is most commonly used in industry to machine precise gratings on metallic substrates. However, in addition to the limitation for generating gratings with small spacing down to subwavelength, the low machining rate of ruling restricts its further adoption in image rendering application. Non-mechanical manufacturing methods are represented by chemical assisted etching/lithography [6] and laser (e-beam, focused ion beam) ablation [7,8]. Although chemical-assisted etching/lithography provides a flexible way of generating 2D microstructures, it is limited in the capacity to texture a continuously curved surface required for concave-convex basso-relievo. Etching wavelength and sub-wavelength are also associated with high cost and special fabrication techniques. Laser (e-beam and focused ion beam) ablation shows excellent performance in terms of structure spatial resolution and surface integrity [9] and has been widely adopted for proof-of-concept studies in micro-structure applications. Nevertheless, the low material removal rate and

* Corresponding author.
E-mail addresses: wangjj11@foxmail.com, jjwang@northwestern.edu (J. Wang), ping.guo@northwestern.edu (P. Guo).

https://doi.org/10.1016/j.precisioneng.2020.03.021
Received 1 February 2020; Received in revised form 26 March 2020; Accepted 26 March 2020
Available online 7 April 2020

high system cost make them undesirable for industrial mass production.

Recently, a cost-effective process based on elliptical vibration cutting has been demonstrated in the structural coloration on metallic substrates [10]. The process utilizes the elliptical vibration of a diamond cutting tip along with a nominal cutting motion to generate overlapping tool trajectories [11]. The machined scallops formed by the tool trajectory represent conjunctive grating-like structures, whose pitch can be controlled down to the near-subwavelength [12]. Through the controlled variation of nominal cutting speed, the grating spacing can be adjusted at each pixel location, resulting in colorized 2-D images based on diffraction effects [13]. Due to its process superiority in flexibility, efficiency and accuracy [14], elliptical vibration cutting can also be used to texture surface structures for an array of breakthrough applications in friction/drag reduction [15,16], wettability enhancement [17], anti-counterfeiting [18], interface medication of lithium battery [19], etc.

In this paper, we demonstrate the combination of surface sculpturing and elliptical vibration texturing to fabricate structurally colored basso-relievo in one-step machining. Here we refer surface sculpturing as the generation of nonperiodic structures, while surface texturing is the generation of periodic structures. The length-scale of the two might have some overlapping, but in general, sculpturing works in the micron-to-millimeter scale, while texturing works in the nano-to-micron scale. Based on the conventional vibration texturing, additional synergistic modulation of both nominal cutting velocity and cutting depth are applied to provide both concave-convex surface topography and structural coloration. New rendering strategies both in the raster scan as well as face turning configurations are presented. In addition, with the dynamic change of nominal depth of cut (*DOC*) in the proposed new process, the grating formation quality will be significantly affected by the proper choice of tool vibration trajectories. Experimental studies are carried out to further the understanding of non-linear effects from interactions between the tool trajectories and workpiece, and to identify the proper process window in terms of vibration trajectories and the *DOC* range.

2. Process principle

2.1. Modulated elliptical vibration texturing

The proposed method, modulated elliptical vibration texturing, machines structurally colored basso-relievo in one-single step with combined sculpturing and texturing operations. It can be mainly ascribed to the synergistic modulation of nominal cutting speed and DOC in elliptical vibration texturing. Fig. 1 shows the schematics of modulated elliptical vibration texturing for both the raster scan and face turning configurations. The modulation of nominal cutting speed is used to generate near-subwavelength grating-type microstructures with controllable spacing distances. The machined grating-type microstructures are able to diffract the visible white light to provide structural coloration. Meanwhile, the modulation of *DOC* is used to adjust the relative height variation of microstructures to provide the concave-convex topography of basso-relievo. By combining the nominal cutting speed and *DOC* modulation simultaneously, structurally colored basso-relievos with stimulating visual effects can be fabricated. It is worth noting that, for a fixed tool nose radius, the grating spacing generated by elliptical vibration texturing is only related to the tool vibration trajectory and cutting velocity, but independent of *DOC*. That is to say, even with different *DOC*, the generated gratings are in principle identical, which is a critical feature to enable the fabrication of basso-relievos with structural colors.

The fundamental of structural coloration in this study is the grating diffraction as shown in Fig. 1(c). According to our previous study and grating diffraction principle [13], for the incident angle $\theta_i = 45°$ and diffractive angle $\theta_k = 0°$ (the observing direction is rightly perpendicular to the machined surface), the relationship between the spacing distance d of grating patterns and light wavelength λ at the second diffraction order can be expressed as:

$$d = 2\sqrt{2}\lambda = \frac{V_c}{f} \tag{1}$$

where V_c and f denote the nominal cutting speed and vibration

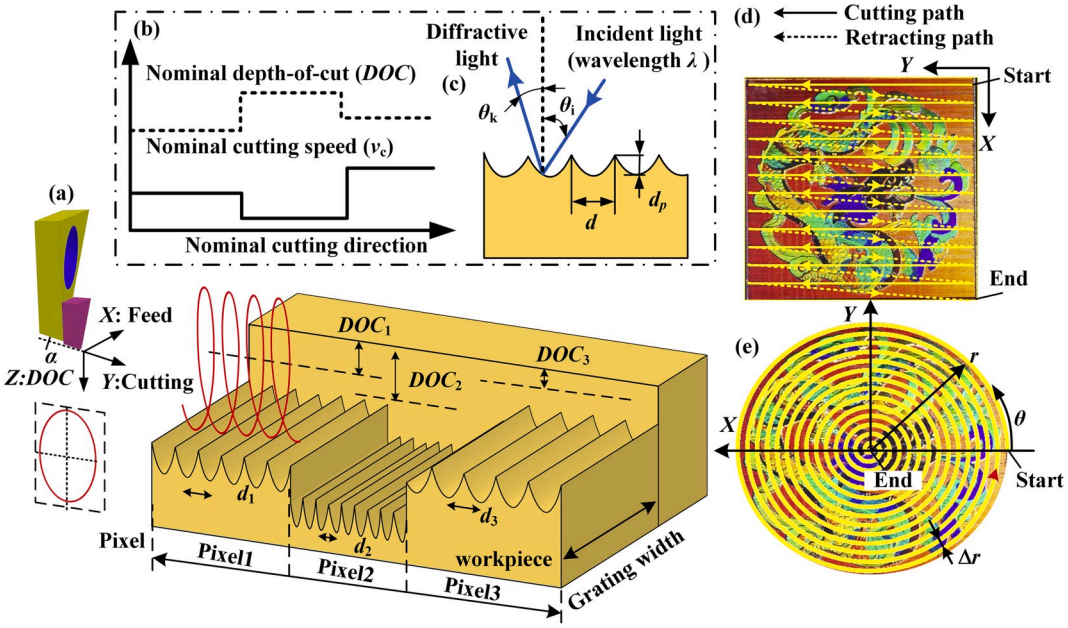

Fig. 1. Illustration of modulated elliptical vibration texturing: (a) process principle; (b) modulation of nominal cutting speed and depth-of-cut (*DOC*); (c) optical diffraction of gratings; (d) raster scan tool path; (e) spiral tool path for face turning.

frequency respectively. For the visible lights with a wavelength of λ ranging from 380 nm to 740 nm, the grating spacing d can be calculated as 1.1 μm to 2.1 μm.

2.2. 3D image rendering strategy with raster scan and face turning configurations

The modulated elliptical vibration texturing can be implemented in the planing setup with a raster scan tool path, as shown in Fig. 1(d). Although the surface colorizing results created through the raster scan setup are promising, it may suffer from the drawback of low machining efficiency. In the raster scan setup, the tool has to perform a retracting action after each cutting pass. The vibration texturing efficiency with the raster scan tool path is significantly restricted due to the tool retracting action. The time wasted can be as large as 50% due to the retracting action for each feed. More seriously, the pre-acceleration and post-deceleration motions outside of the cutting region could further reduce its machining efficiency and affect the cutting stability.

To improve the machining efficiency, we also propose a face turning configuration to implement the modulated elliptical vibration texturing, as shown in Fig. 1(e). The tool path of face turning is an equidistant spiral, which can be described by

$$r_0 - \frac{\theta}{2\pi}\cdot\Delta r = r \tag{2}$$

where r is the radial position of tool; r_0 is the starting radius; Δr is the spiral pitch; and θ is the accumulated angle of spindle rotation during the process. By substituting the disrupted raster scan path by a continuous tool path, the face turning operation can eliminate the time-wasting retraction motion and achieve a more stable and continuous cut.

For both raster scan and face turning, the rendering strategy of colored basso-relievos from a 3D image is illustrated in Fig. 2. The colored 3D image can be developed according to the customized requirement of visual effects using a professorial software-JD painting. The colored 3D image consists of both the information of relative height variation and colors of each pixel. Using JD painting, the height variation information can be exported as a 2D grayscale image, while color information can be exported as a 2D colored image.

For a raster scan, the original image is segmented into pixels with the same size along the scan path. A Cartesian coordinate system XY is established on the original image, where (X_N, Y_N) is the coordinate of the Nth pixel. The grayscale image can be expressed using a sequence $Gray$ (X_N, Y_N), which is used to control the modulation of depth-of-cut through a function g_1. On the other hand, the hue axis of the color information (HSV) of the 2D colored image can be expressed using a sequence $Hue(X_N, Y_N)$ [13], which is used to control the modulation of nominal cutting speed through a function g_2. The tool modulation control functions g_1 and g_2 can be expressed as:

$$\begin{cases} g_1 : DOC(X_N, Y_N) = DOC_{\max}(1 - Gray(X_N, Y_N)/255) \\ g_2 : V_c(X_N, Y_N) = \mathbf{2}\sqrt{2}\cdot\lambda(Hue(X_N, Y_N))\cdot f \end{cases} \tag{3}$$

where DOC (X_N, Y_N) and V_c (X_N, Y_N) are the depth-of-cut and nominal cutting speed of Nth pixel; $DOC_{\max}$ is the DOC range, namely the maximum height variation of basso-relievo. For $f = 1$ kHz, the nominal cutting speed V_c range can be determined to be from 1.2 to 2.0 mm/s, which characterizes the writing speed for the sculpturing and colorizing process. In Eq. (2), $\lambda(Hue)$ establishes the relationship between the hue of images and the wavelength of diffractive light [13] as:

$$\lambda(Hue) = \begin{cases} -0.26\cdot Hue + 0.64 Hue \in [0, 0.9) \\ 0.7\cdot Hue + 0.01 Hue \in [0.9, 1) \end{cases} \tag{4}$$

For face turning, the spiral tool path can also be segmented into pixels with the same size. A polar coordinate system is established on the original image, where (r_N, θ_N) is the coordinate of the Nth pixel. The corresponding gray and color sequences $Gray$ (r_N, θ_N) and Hue (r_N, θ_N) in the polar coordinate system can be obtained from the gray and color sequences in the Cartesian coordinate system through simple coordinate system transformation and linear interpolation and rounding:

$$\begin{cases} X_N = r_N \cos(\theta_N) \\ Y_N = r_N \sin(\theta_N) \end{cases} \tag{5}$$

Then the pixel by pixel control equations g_1 and g_2 for DOC and nominal cutting speed modulation can be expressed as:

$$\begin{cases} g_1 : DOC(r_N, \theta_N) = DOC_{\max}(1 - Gray(r_N, \theta_N)/255) \\ g_2 : V_c(r_N, \theta_N) = \mathbf{2}\sqrt{2}\cdot\lambda(Hue(r_N, \theta_N))\cdot f \end{cases} \tag{6}$$

where DOC (r_N, θ_N) and V_c (r_N, θ_N) are the depth-of-cut and nominal cutting speed of the Nth pixel in face turning. Different from that in the raster scan, the modulation of nominal cutting speed in face turning is provided by the spindle rotation. The spindle rotating speed ω_N for the Nth pixel in face turning has to be adjusted according to radial position r_N of the tool through

$$\omega_N = \frac{V_c(r_N, \theta_N)}{r_N} \tag{7}$$

3. Non-linear interactions between tool vibration and workpiece

The process parameters, such as the nominal cutting speed, DOC and elliptical trajectory have critical effects on the surface generation quality of gratings. For the high-quality sculpturing of colored basso-relievo, the nonlinear interactive effects of process parameters should be carefully explored to identify the proper process window. In the newly proposed process, the nominal cutting speed and DOC are synergistically modulated. However, the dynamic change of DOC in the basso-relievo

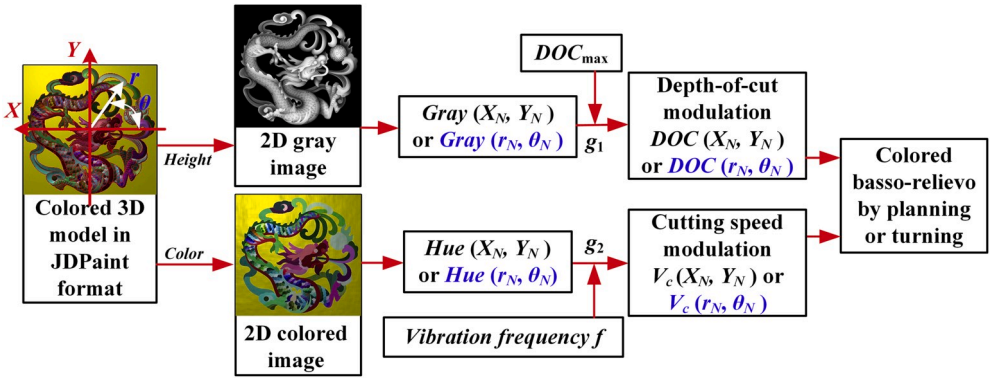

Fig. 2. 3D image rendering process for both raster scan and face turning.

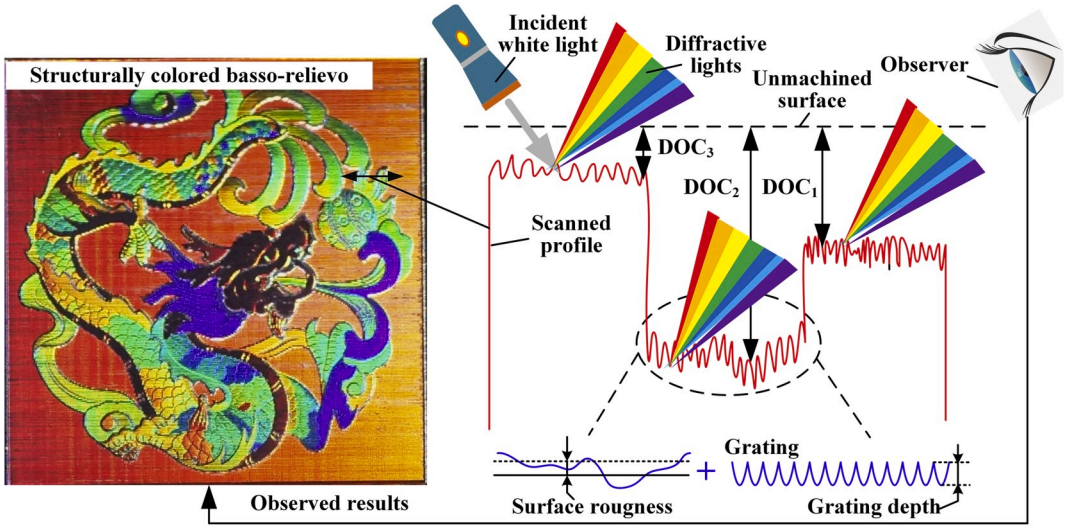

Fig. 3. Performance indices characterizing the surface generation quality: grating depth and surface roughness.

sculpturing might violate the optimum generation condition of grating-type microstructures as shown in Fig. 3. The tool-workpiece interactions need to be systematically investigated to achieve both the high-quality grating generation for better structural coloration; and 2) large *DOC* adjustment range for more distinctive concave-convex effects.

3.1. Design of inclined grooving experiments

The surface quality of machined gratings is a crucial factor that affects the optical performance of rendered images. In order to evaluate the surface quality of grating patterns, the grating depth (diffraction efficiency) and surface roughness (reflection efficiency) are used as the characterizing indices as described in Fig. 3. The grating depth is the maximum height variation of generated periodic microstructures, while the surface roughness is a relatively macro height variation of the machined surface by filtering out the grating profiles. The effects of process parameters on these two surface quality indices can be assessed through an inclined grooving test.

Inclined grooving experiments with elliptical tool vibrations were conducted on ultra-machinable 360 brass (*Mcmaster-carr, USA*) to evaluate the effects of process parameters on the surface quality of generated grating patterns. The experimental setup is shown in Fig. 4 with the detailed process parameters summarized in Table 1. A diamond tool with a nose radius of 600 μm, a rake angle of 0° and a clearance angle of 20° was used for cutting. As demonstrated in Fig. 4(a), the cutting path has a relative inclination angle of 10 ìm/mm with respect to

Table 1
Experimental condition for process investigation (f = 1000 Hz).

Trajectory No.	Descriptions	Nominal cutting speed V_c (mm/s)
①	a = 3 μm, b = 1 μm, θ = 0°	1, 1.5, 2, 3
②	a = 3 μm, b = 1 μm, θ = 45°	1, 1.5, 2, 3
③	a = 3 μm, b = 1 μm, θ = 90°	1, 1.5, 2, 3
④	a = 3 μm, b = 1 μm, θ = 135°	1, 1.5, 2, 3
⑤	a = 1 μm, b = 1 μm, θ = 0°	1, 1.5, 2, 3
⑥	a = 2 μm, b = 2 μm, θ = 0°	1, 1.5, 2, 3
⑦	a = 3 μm, b = 3 μm, θ = 0°	1, 1.5, 2, 3

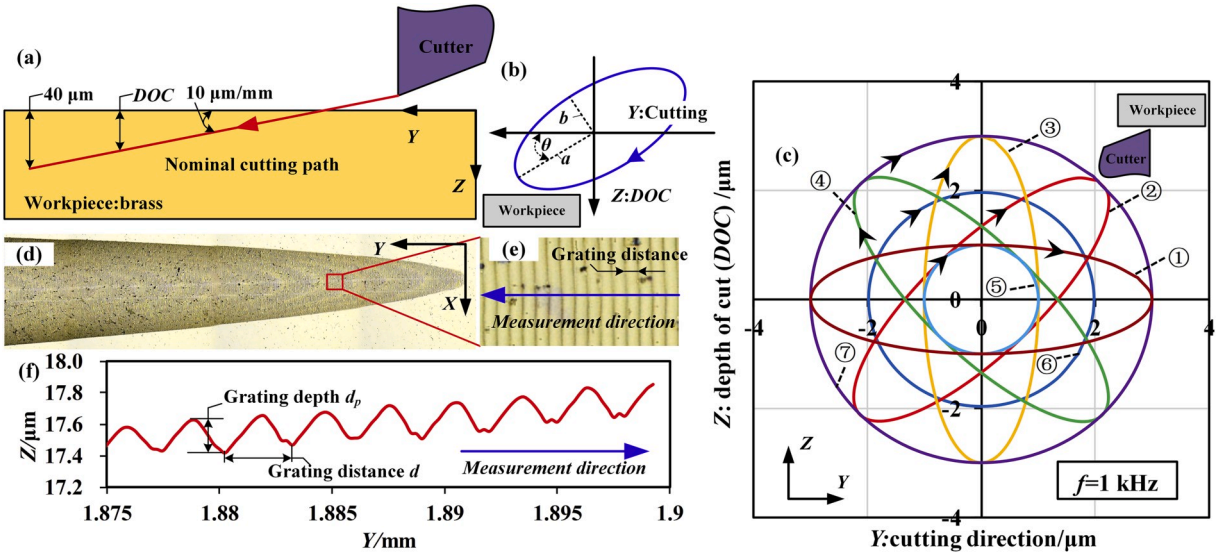

Fig. 4. Illustration of grooving experiments for process parameter determination of basso-relievo sculpturing. (a) grooving path; (b) definition of elliptical trajectory; (c) applied elliptical trajectories; (d) grooved surface; (e) enlarged surface morphology; (f) grating profile.

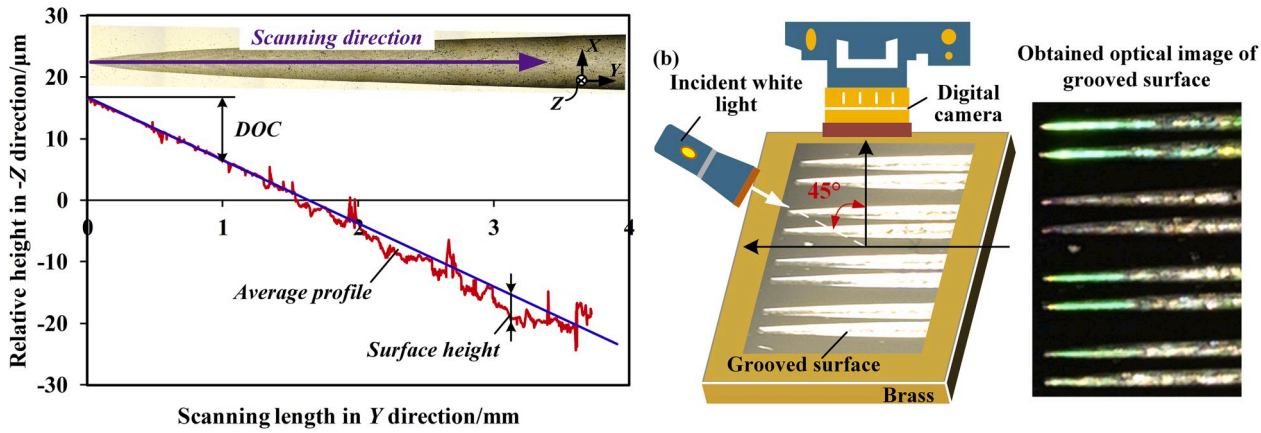

Fig. 5. (a) Typical cross-sectional profile of a grooved surface; (b) optical photos taken with white light illumination.

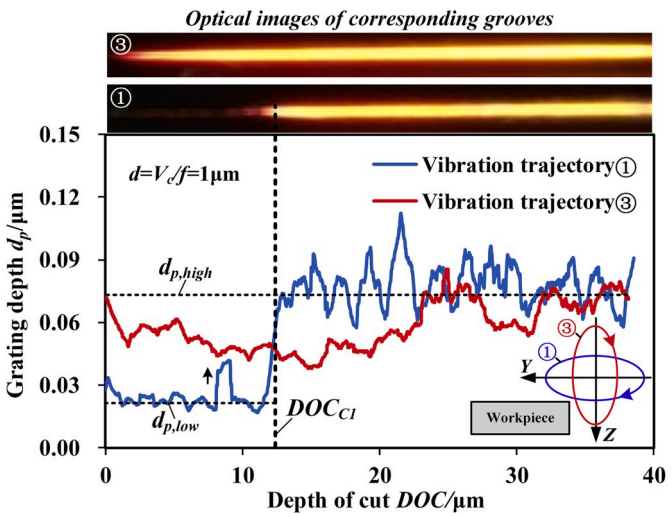

Fig. 6. Typical grating depth variation with increasing *DOC*.

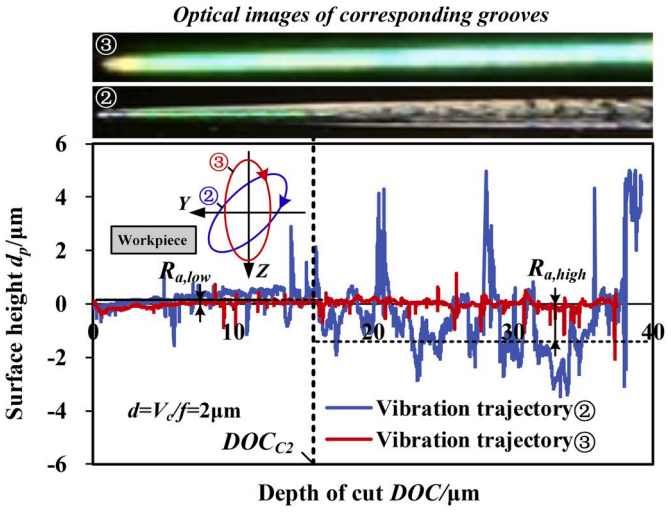

Fig. 7. Surface roughness variation with increasing *DOC*.

the workpiece surface. The maximum grooving *DOC* was set as 40 μm.

Seven sets of elliptical vibration trajectories were utilized with different semi-major axis a and semi-minor axis b and orientation angle θ as defined in Fig. 4(b). The adopted elliptical trajectories with a vibration frequency f of 1 kHz are demonstrated in Fig. 4(c). The nominal cutting speeds were set as 1, 1.5, 2, 3 mm/s in the grooving experiments to control the grating spacing distances as 1, 1.5, 2 and 3 μm. The grooved surfaces with vibration texturing were observed and measured using a 3D laser confocal microscope (*OLS5000, Olympus, USA*). Fig. 4 (d) and (e) show an image of the grooved surface and its locally enlarged morphology, from which the periodic grating-type microstructures can be identified. The cross-sectional profile of the generated gratings in Fig. 4(e) is shown in Fig. 4(f), from which the grating depth d_p can be obtained.

The effects of *DOC* on the grating depth and surface roughness for different nominal cutting speed and elliptical trajectory can be quantified from the cross-sectional profiles of the measured grooved surface. Fig. 5 shows a typical cross-sectional profile of the grooved surfaces and their optical images. As shown in Fig. 5(a), with the increase of scanning length from left to right, the average depth of grooved surface increases linearly. The average profile of machined groove can be fitted as a linear line. Then, the grating depth and relative surface height with respect to the average profile for different *DOC* can be obtained with represented results shown in Fig. 6 and Fig. 7. In addition, the optical photos taken with white light illumination are also used to help estimate the surface quality of generated gratings as shown in Fig. 5(b).

3.2. Effects of depth-of-cut (DOC) on grating generation

The change of *DOC* may have a decisive influence on the grating depth. The variation of grating depth with the increase of *DOC* with the corresponding diffractive colored images of machined grooves for two typical vibration trajectories is shown in Fig. 6. It can be seen that, for vibration trajectory ①, there exists a sharp increase of grating depth from an average value of $d_{p,low}$ to $d_{p,high}$ when the *DOC* exceeds a lower limit value DOC_{C1}. When $DOC < DOC_{C1}$, the depth of generated grating is too small to provide sufficient diffractive color. In other words, only when the *DOC* increases up to the lower limit value DOC_{C1}, the white light can be efficiently diffracted. This phenomenon could be attributed to the ploughing effects in the cutting process. When the *DOC* is below its lower limit, too much ploughing happens that restricts the clear formation of grating structures. However, for vibration trajectory ③, there is no obvious evidence that the lower limit of *DOC* exists. The white light can be efficiently diffracted by the gratings generated with vibration trajectory ③ for all values of *DOC* from 0 to 40 μm. This indicates that the vibration trajectory should have significant effects on the surface generation quality of gratings.

In addition to the grating depth, the *DOC* may also influence the surface roughness of machined grooves. The variation of surface roughness with the increase of *DOC* for two typical vibration trajectories

and the corresponding diffractive colored images of machined grooves are shown in Fig. 7. It can be seen that, for vibration trajectory ②, there exists a sudden deterioration of surface quality, when the *DOC* exceeds an upper limit value DOC_{C2}. When $DOC > DOC_{C2}$, the surface roughness of generated grating patterns increases from $R_{a,low}$ to $R_{a,high}$. Under the circumstances, the machined surface is too rough to reflect and diffract white lights. To ensure the white light be efficiently reflected and diffracted, the *DOC* should be kept below its upper limit value DOC_{C2}. This phenomenon could be attributed to the instability in the cutting process. When the *DOC* exceeds its upper limit, the large impact cutting force might trigger the instability resulting in the deterioration of surface quality. In contrast, for vibration trajectory ③, the upper limit of *DOC* doesn't exist. The white light can be efficiently reflected and diffracted by the gratings machined with vibration trajectory ③ for all values of *DOC* from 0 to 40 μm. This example further demonstrates that the vibration trajectory significantly affects the surface quality of gratings.

In summary, the above two exemplary cases in terms of the effects of *DOC* on the grating depth and surface roughness defines the lower limit and the upper limit of the applicable *DOC*. The applicable *DOC* is bounded by its lower limit and the upper limit. Hence, for the high-quality basso-relievo sculpturing, we would like to extend the range of *DOC* defined by the lower limit DOC_{C1} and the upper limit DOC_{C2}.

3.3. Effects of elliptical vibration trajectory on grating generation

The elliptical trajectory also has crucial effects on the surface generation quality of gratings. To quantitatively evaluate the effects of elliptical vibration trajectory on grating generation quality, the characterizing indices of surface quality including grating depths: $d_{p,low}$, $d_{p,high}$, surface roughness: $R_{a,low}$, $R_{a,high}$ and critical DOC:DOC_{C1}, DOC_{C2} were obtained for all designed experimental conditions. The excavated data of characterizing indices are shown in Fig. 8 and Fig. 9 to demonstrate the effects of vibration trajectory.

The elliptical trajectory significantly affects the lower limit and upper limit of DOC. As shown in Fig. 8, only trajectory No.②③④ are applicable in terms of relatively large grating depth, since they have a lower limit of *DOC* (DOC_{C1}) with zero value. However, if considering the surface roughness of machined surfaces, trajectory No.② is excluded from the applicable trajectories group, due to the obvious degradation of surface quality as shown in Fig. 9. This could result from the sharp increase of chip thickness during the vibration cutting process with trajectory No.②, which has a 45° orientation angle. As demonstrated in our previous study regarding silicon cutting [20], trajectory No.② is not beneficial to improve the surface integrity of machined surfaces due to undesired chip thickness variation. Hence, considering both the surface roughness and grating depth, trajectory No. ③ and ④ are acceptable.

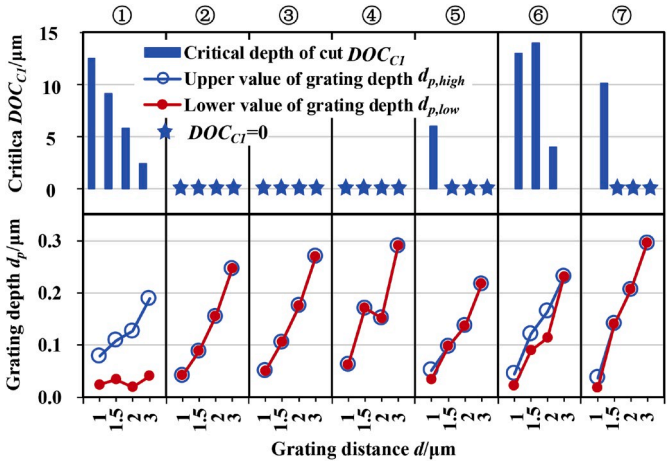

Fig. 8. Effects of vibration trajectories on grating depth.

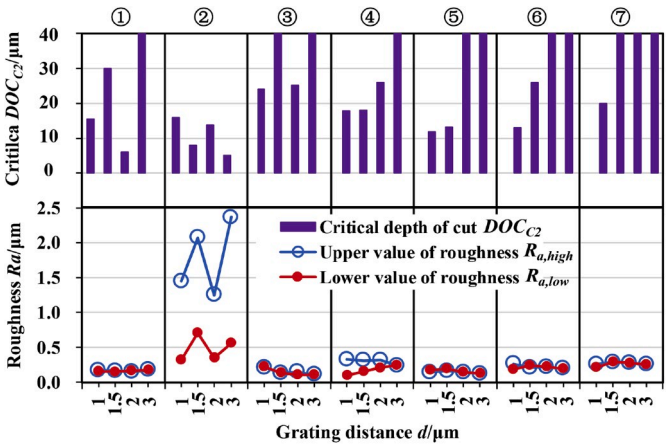

Fig. 9. Effects of vibration trajectories on surface roughness.

But considering that trajectory No. ③ can achieve larger DOC_{C2}, it is slightly better than trajectory No. ④ for the high-quality fabrication of structurally colored basso-relievo.

In summary, for sculpturing colored basso-relievo on ultra-machinable 360 brass with grating spacing distances of 1–3 μm, the best elliptical trajectory is an uninclined ellipse with $a = 1$ μm, $b = 3$ μm, which can achieve maximum practicable DOC>20 μm without deteriorating the surface quality of generated grating patterns.

4. Vibration sculpturing results

4.1. Sculpturing and measurement setup

The sculpturing tests were performed on an ultra-precision machine center (*Nanoform X, Precitech, USA*) with three linear axes (XYZ axis) and a spindle (C axis). The machine setup with the coordinate system definition is shown in Fig. 10. The brass workpiece is mounted on the spindle through a vacuum chuck. The workpiece surface is pre-turned before basso-relievo sculpturing to ensure a flat and perfectly aligned surface. A non-resonant 2-D vibration generator, which has been previously developed with a frequency bandwidth up to 2 kHz and a stroke space of 15 μm × 16 μm, is used to generate elliptical vibration [20]. Tool vibration signals are generated using a *Labview* program and outputted through a high-speed data acquisition card (*National Instruments*, USA) and amplified by a two-channel piezo amplifier (*PX200, PiezoDrive, Australia*). The cutting tool is mounted on the *Y* slide on top of the *Z* slide. The cutting motion with the controlled velocity modulation is provided by the *Y*-axis motion with the position-velocity-time interpolation method in the raster-scan configuration; while in the face turning configuration, the primary cutting motion is provided by the spindle rotation. The *Z* slide dynamically controls the *DOC* for surface sculpturing. The *X*-axis stage carries the spindle assembly to provide the cross-feed motion.

Two optical measurement systems are set up to capture the visual appearance of structurally colored basso-relievos, as illustrated in Fig. 11. Since the machined grating structures are always perpendicular to the cutting direction. The rendered images are observed in the in-plane mount with an incident white light beam at 45° and an observing direction perpendicular to the machined surface. Images are taken by a digital camera mounted with a fixed focal length lens (*Sony, Japan*). For the turned samples, the gratings are along the radial direction of the round workpiece, whose direction varies for each angular position. A ring light is used to illuminate the workpiece to achieve full-field diffraction effects, while the camera is mounted in the perpendicular direction to the machined surface. In addition, the machined surface profiles are obtained with a 3D laser confocal microscope (*OLS5000, Olympus, Japan*).

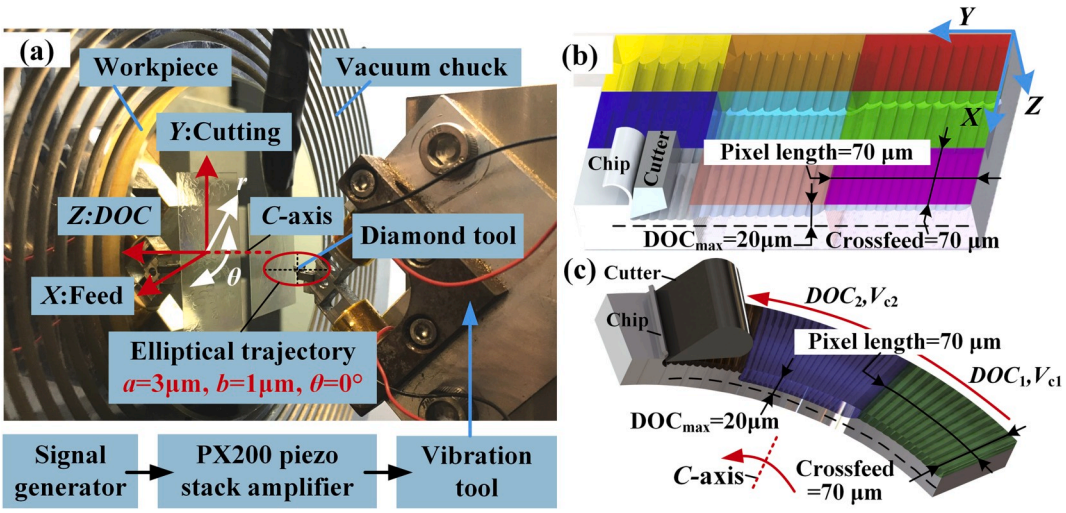

Fig. 10. (a) Experimental setup for modulated elliptical vibration texturing; process parameters for (b) raster scan and (c) face turning.

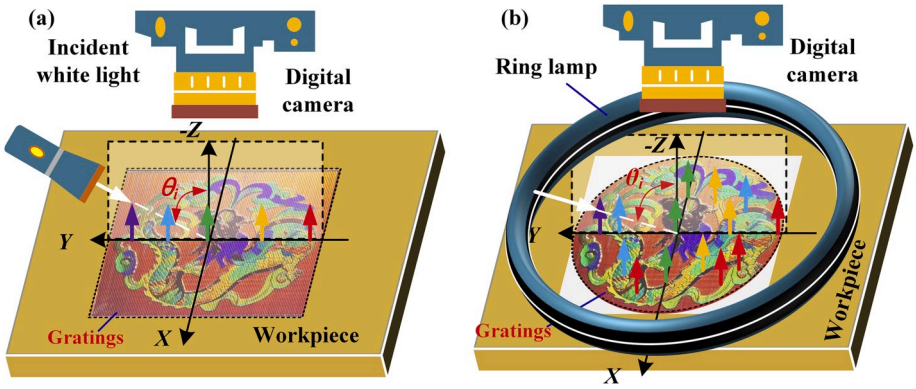

Fig. 11. Optical measurement system for (a) raster-scanned and (b) face-turned basso-relievos.

Table 2
Information of images to be rendered.

Image label	Geometric dimension	Render strategy
Chinese dragon	25 mm × 25 mm	Raster scan
Chinese dragon	Φ 25 mm	Face turning
Landscape	20 mm × 35 mm	Raster scan
Owl	20 mm × 30 mm	Raster scan
Tiger	20 mm × 27 mm	Raster scan

4.2. Experimental conditions for sculpturing tests

As described in the rendering strategy section, modulated elliptical texturing is carried out to render several 3D images (see Table 2) with both a raster scan tool path in a planing configuration and an equidistant spiral tool path in a face turning setup. Fig. 10(b) and (c) show the process parameters for the configurations of raster scan and face turning respectively. The pixel size for all sculpturing tests is set to 70 μm × 70 μm, so the cross-feed is maintained at 70 μm, while the cutting velocity is adjusted in a range of 1.1–2.1 mm/s at a fixed distance of 70 μm accordingly. The maximum variation range of *DOC* (DOC_{max})for every pixel is set to 20 μm. The elliptical vibration ($a = 1$ μm, $b = 3$ μm, $\theta = 0°$, $f = 1$ kHz) is generated on a single crystal diamond insert (*Contour Fine Tooling, UK*), which has a nose radius of 600 μm, a rake angle of 0°, and a clearance angle of 20° in all sculpturing experiments.

4.3. Results of structurally colored basso-relievo

A design of Chinese dragon is rendered in a raster scan tool path with the recorded visual appearance compared in Fig. 12. In Fig. 12(a), conventional elliptical vibration texturing is first applied to achieve a structurally colored image without the modulation of *DOC*. Fig. 12(b) shows the basso-relievo sculptured result without structural colors. Fig. 12(c) demonstrates the colored basso-relievo machined by the proposed modulation vibration texturing. Similar results of basso-relievo have also been demonstrated on hardened steel in Suzuki et al.'s study [21] through an amplitude control method in elliptical vibration cutting. In their study, the elliptical vibration is utilized to improve the material machinability through its unique capacity of chip thickness reduction, rather than to generate grating-type microstructures. Hence, their results only have the concave-convex visual effects with no structural colors. In this study, the newly proposed process combines the elliptical vibration to create gratings for structural colors and the *DOC* modulation to generate concave-convex surfaces. Compared with the results in Fig. 12(a) and (b) that only show the structural coloration or relief image, the colored basso-relievo is more eye-catching with refined details. For the inset in Fig. 12(c), the microscopic view at the center of the basso-relievo is presented in Fig. 12 (d). The detailed surface profiles both measured along the cross-feed (Profile 1) and cutting (Profile 2) directions are presented in Fig. 12 (e). Concave-convex surface features are successfully captured and

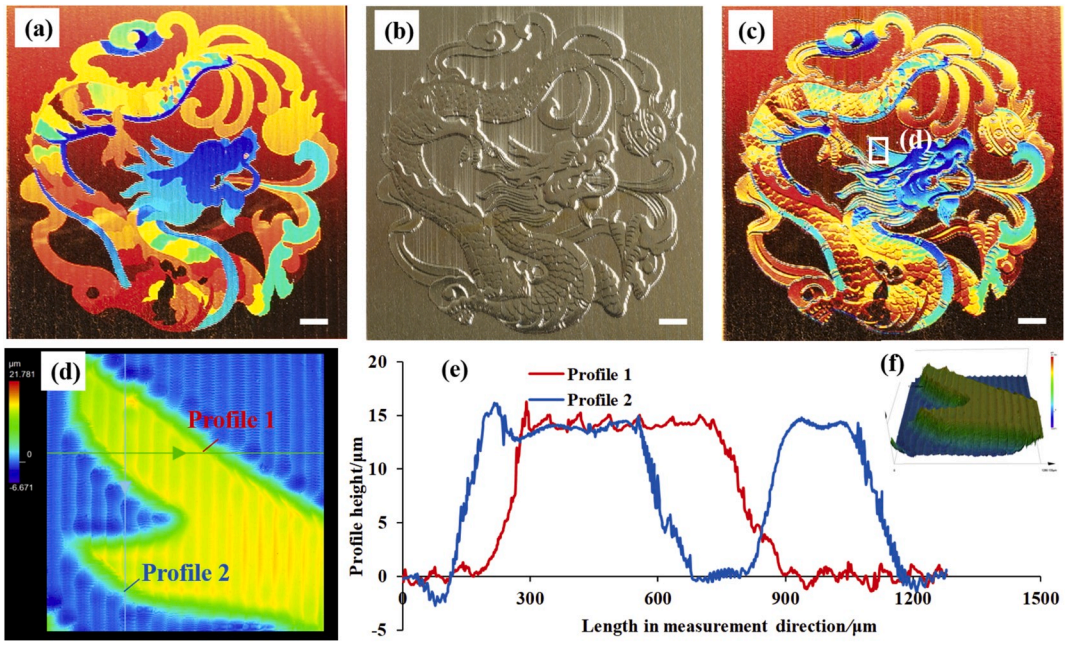

Fig. 12. Machined results of a Chinese dragon design (scale bar = 2 mm). Optical images of textured samples for (a) elliptical vibration texturing without DOC modulation ($\theta_i = 45°$); (b) with DOC modulation ($\theta_i = 0°$); and (c) with DOC modulation ($\theta_i = 45°$). (d) surface profile measurement of the dragon horn; (e) cross-sectional profiles along the cutting and cross-feed directions; (f) surface height map.

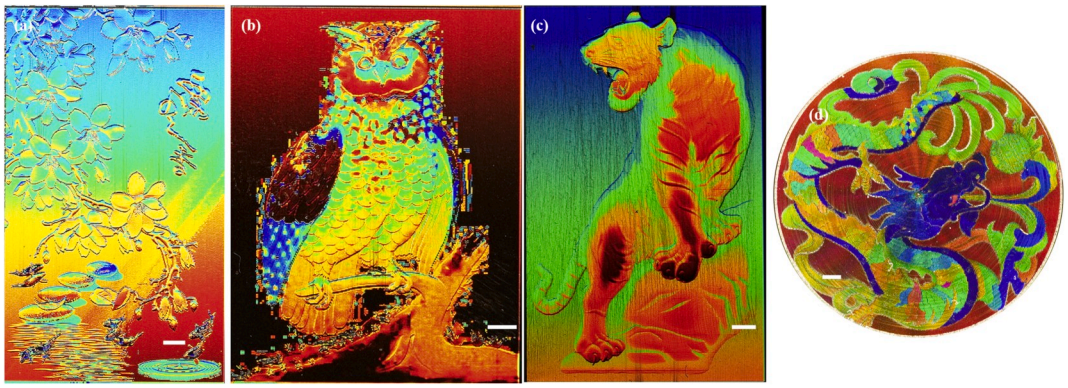

Fig. 13. Results of basso-relievo on brass samples (scale bar = 2 mm): (a) landscape; (b) owl; (c) tiger with a raster-scan tool path; and (d) Chinese dragon from the face turning configuration.

further illustrated in Fig. 12(f). In addition, more results of structurally colored basso-relievo are demonstrated in Fig. 13. These results have verified the efficacy of the proposed approach to fabricate colored basso-relievos, which should be able to achieve even higher machining efficiency with an ultrasonic elliptical vibration tool [22]. The successful fabrication of structurally colored basso-relievo also demonstrates the unique capacity of the proposed process in freeform surface texturing. This could enable its unique application potentials compared with other surface texturing processes.

Compared with established techniques for structurally surface colorizing such as femtosecond laser structuring [23] and laser interference patterning [24,25], the proposed modulated vibration texturing process can realize one-step machining for colored basso-relievo fabrication by combining surface sculpturing and texturing with a single setup. It might be possible that the laser-based process can also be used for surface sculpturing by improving the power input to enhance the material removal volume. However, the surface quality and material removal volume of laser-based process cannot be achieved simultaneously. Hence, the process has to be divided into two discrete steps including surface sculpturing (utilizing micro-milling for example) and surface texturing (by laser-based process) [26]. The separation of two micro-machining steps not increases the manufacturing time and costs, but also brings more technical challenges of real-time focusing due to the variation of surface height of sculptured surfaces.

5. Conclusions

This study proposes a one-step fabrication method for structurally colored basso-relievo with modulated elliptical vibration texturing. The modulation of nominal cutting speed controls the generated gratings spacings to provide diffractive structural coloration. In the meantime, the synergistic modulation of DOC controls the relative height variations of generated gratings to provide concave-convex topography. Grooving experiments were conducted on brass workpieces to understand the nonlinear interactions between tool and workpiece. The grating depth and surface roughness were utilized to characterize the surface quality of generated grating patterns. The process window in terms of vibration trajectory and *DOC* range was identified based on the above cutting mechanism study. The following conclusions can be drawn.

(1) New 3D image rendering strategy for both raster scan and face turning configurations have been presented. The face turning setup utilizes an equidistant spiral tool path. It is able to improve the image rendering efficiency by eliminating the time-wasting tool retracting action over the raster scan.
(2) For the high-quality basso-relievo sculpturing, the applicable *DOC* should be bounded by a lower limit and upper limit. This results from the inverse effects of *DOC* on the grating depth and surface roughness. The applicable range of *DOC* is significantly dependent on the elliptical trajectory. The best elliptical vibration trajectory is an uninclined ellipse with amplitudes of 1 μm and 3 μm in cutting and *DOC* directions respectively. It can achieve the maximum upper limit of *DOC*>20 μm without deteriorating the surface quality of generated grating patterns.
(3) Sculpturing tests with a line writing speed of 1.1–2.1 mm/s on brass verified the efficacy of the proposed process. It can fabricate structurally colored basso-relievos in one-step machining. The speed can be potentially improved 10-30 times by adopting an ultrasonic vibration cutting tool. Compared with the machined results with only structural colors or basso-relievo, the structurally colored basso-relievo demonstrates a more eye-catching visual appearance with refined details.

Declaration of competing interest

The authors declare that they have no known competing financial interests or personal relationships that could have appeared to influence the work reported in this paper.

Acknowledgments

This research was supported by the start-up fund from McCormick School of Engineering, Northwestern University, Evanston, IL, USA; and the Innovation and Technology Fund, Hong Kong, #ITS/076/17. This work made use of the MatCI Facility which receives support from the MRSEC Program (NSF DMR- 1720139) of the Materials Research Center at Northwestern University.

References

[1] Tunc LT. Smart tool path generation for 5-axis ball-end milling of sculptured surfaces using process models. Robot Cim-Int Manuf 2019;56:212–21.
[2] Williams TL, Senft SL, Yeo J, Martín-Martínez FJ, Kuzirian AM, Martin CA, Dibona CW, Chen C, Dinneen SR, Nguyen HT, Gomes CM, Rosenthal JJC, Macmanes MD, Chu F, Buehler MJ, Hanlon RT, Deravi LF. Dynamic pigmentary and structural coloration within cephalopod chromatophore organs. Nat Commun 2019;10(1):1004.
[3] Sun J, Bhushan B, Tong J. Structural coloration in nature. RSC Adv 2013;3(35):14862–89.
[4] Andreeva YM, Luong VC, Lutoshina DS, Medvedev OS, Mikhailovskii VY, Moskvin MK, Odintsova GV, Romanov VV, Shchedrina NN, Veiko VP. Laser coloration of metals in visual art and design. Opt Mater Express 2019;9(3):1310–9.
[5] Zhao Y, Zhao Y, Hu S, Lv J, Ying Y, Gervinskas G, Si G. Artificial structural color pixels: a review. Materials 2017;10(8):944.
[6] Wu H, Jiao Y, Zhang C, Chen C, Yang L, Li J, Ni J, Zhang Y, Li C, Zhang Y, Jiang S, Zhu S, Hu Y, Wu D, Chu J. Large area metal micro-/nano-groove arrays with both structural color and anisotropic wetting fabricated by one-step focused laser interference lithography. Nanoscale 2019;11(11):4803–10.
[7] Müller F, Kunz C, Gräf S. Bio-inspired functional surfaces based on laser-induced periodic surface structures. Materials 2016;9(6):476.
[8] Rosenkranz A, Hans M, Gachot C, Thome A, Bonk S, Mücklich F. Direct laser interference patterning: tailoring of contact area for frictional and antibacterial properties. Lubricants 2016;4(1):2.
[9] Müller DW, Fox T, Grützmacher PG, Suarez S, Mücklich F. Applying ultrashort pulsed direct laser interference patterning for functional surfaces. Sci Rep-UK 2020;10(1):1–14.
[10] Yang Y, Pan Y, Guo P. Structural coloration of metallic surfaces with micro/nano-structures induced by elliptical vibration texturing. Appl Surf Sci 2017;402:400–9.
[11] Geng D, Liu Y, Shao Z, Zhang M, Jiang X, Zhang D. Delamination formation and suppression during rotary ultrasonic elliptical machining of CFRP. Compos B Eng 2020;183:107698.
[12] Guo P, Ehmann KF. An analysis of the surface generation mechanics of the elliptical vibration texturing process. Int J Mach Tool Manufact 2013;64:85–95.
[13] Yang Y, Guo P. Global tool path optimization of high-resolution image reproduction in ultrasonic modulation cutting for structural coloration. Int J Mach Tool Manufact 2019;138:14–26.
[14] Geng D, Liu Y, Shao Z, Lu Z, Cai J, Li X. Delamination formation, evaluation and suppression during drilling of composite laminates: a review. Composite Structures 2019;216:168–86. https://doi.org/10.1016/j.compstruct.2019.02.099.
[15] Zhang J, Zhang J, Rosenkranz A, Suzuki N, Shamoto E. Frictional properties of surface textures fabricated on hardened steel by elliptical vibration diamond cutting. Precis Eng 2019;59:66–72.
[16] Yeung CS, Yang Y, Du H, Wang J, Guo P. Friction reduction performance of microstructured surfaces generated by nonresonant modulation cutting. P I Mech Eng C-J Mec 2019;233(12):4120–7.
[17] Yuan Y, Zhang D, Jing X, Ehmann KF. Freeform surface fabrication on hardened steel by double frequency vibration cutting. J Mater Process Technol 2020;275:116369.
[18] Guo P, Yang Y. A novel realization of diffractive optically variable devices using ultrasonic modulation cutting. CIRP Ann - Manuf Technol 2019;68(1):575–8.
[19] Zhang X, Wang QJ, Harrison KL, Roberts SA, Harris SJ. Pressure-driven interface evolution in solid-state lithium metal batteries. Cell Reports Physical Science 2020;1(2):100012.
[20] Wang J, Liao W, Guo P. Modulated ultrasonic elliptical vibration cutting for ductile-regime texturing of brittle materials with 2-D combined resonant and non-resonant vibrations. Int J Mech Sci 2019;170:105347.
[21] Suzuki N, Yokoi H, Shamoto E. Micro/nano sculpturing of hardened steel by controlling vibration amplitude in elliptical vibration cutting. Precis Eng 2011;35(1):44–50.
[22] Zhang J, Zhang J, Cui T, Hao Z, Al Zahrani A. Sculpturing of single crystal silicon microstructures by elliptical vibration cutting. J Manuf Process 2017;29(Supplement C):389–98.
[23] Zhang C, Yao J, Liu H, Dai Q, Wu L, Lan S, Trofimov VA, Lysak TM. Colorizing silicon surface with regular nanohole arrays induced by femtosecond laser pulses. Opt Lett 2012;37(6):1106–8.
[24] Voisiat B, Wang W, Holzhey M, Lasagni AF. Improving the homogeneity of diffraction based colours by fabricating periodic patterns with gradient spatial period using Direct Laser Interference Patterning. Sci Rep-uk 2019;9(1):1–9.
[25] Lasagni AF, Gachot C, Trinh KE, Hans M, Rosenkranz A, Roch T, Eckhardt S, Kunze T, Bieda M, Günther D, Lang V, Mücklich F. Direct laser interference patterning, 20 years of development: from the basics to industrial applications. In: Laser-based micro-and nanoprocessing XI. San Francisco, United States: SPIE; 2017. 2017. 10092 1009211.
[26] Lang V, Madelung A, Alamri S, Steege T, Krupop B, Aguilar AI, Kunze T, Lasagni AF. High-throughput direct laser interference patterning: new configurations and applications. In: Laser-based micro-and nanoprocessing XIV. San Francisco, United States: SPIE; 2020. 11268 112680T.